Journal of Materials Chemistry

Cite this: *J. Mater. Chem.*, 2011, **21**, 3183

www.rsc.org/materials

PAPER

Controlled synthesis of ZnO spindles and fabrication of composite photoanodes at low temperature for quasi-solid state dye-sensitized solar cells

Yantao Shi,† Haopeng Dong,† Liduo Wang,* Chun Zhan, Rui Gao and Yong Qiu

Received 2nd November 2010, Accepted 23rd November 2010
DOI: 10.1039/c0jm03742g

In this paper, by altering reactants concentration, ZnO spindles with different sizes were controllably prepared through a fast precipitation process in aqueous solution. Some important characteristics such as specific area, macropore structure, light scattering and electron transport properties of the photoanodes were systematically investigated. The results showed that photoanodes composed of small-sized ZnO spindles had a larger specific area for dye-loading, while the large-sized ZnO spindles had more efficient light scattering and electron transport properties. Furthermore, to combine the advantages of different sized ZnO particles, composite photoanodes were fabricated by mixing together ZnO spindles of different sizes. Compared with the dye sensitized solar cells (DSCs) using photoanodes with single-sized ZnO spindles, the devices based on composite photoanodes showed a higher short-circuit photocurrent density without obvious decrease in open-circuit voltage and fill factor. As a result, photovoltaic performances of the DSCs were improved remarkably.

1. Introduction

Featuring lower production cost and simpler manufacturing process, dye-sensitized solar cells (DSCs) have been considered as a potential alternative to traditional p-n junction solar cells.[1,2] As a key component of DSCs, porous photoanodes have significant influence on the device's photovoltaic performance. Compared with commonly used TiO_2 photoanodes, ZnO photoanodes have been intensively investigated due to its similar bandgap, easier synthesis process and higher electron mobility.[3–7] In the field of ZnO photoanodes, orderly structured ZnO photoanodes with one-dimensional structures perpendicular to the substrate have always been of research interest, such as nanotubes, nanorods, nanowires, *et al.* In these orderly structured ZnO photoanodes, although charge transport routes are shortened and photoinduced electrons can be more easily collected, conversion efficiencies of corresponding devices are not as high as expected.[8–13] In fact, for a highly performed ZnO porous photoanode, not only electron transport properties in the photoanode but also other factors should be paid attention to simultaneously, such as dye-loading,[14,15] light-scattering,[16–19] pore-structure,[20–22] *et al.* DSCs based on composite structures have shown higher conversion efficiencies than those based on orderly structured ones, in which sufficient dye-loading and light scattering could be obtained simultaneously by those particles with different sizes.[23–28] For example, Cao *et al.* fabricated a hierarchically structured ZnO photoanode that was composed of polydisperse ZnO aggregates made up of nano-sized particles, the primary nano-sized particles and their secondary larger-sized spherical aggregates contributed to the dye-loading and light scattering, respectively, compared to ZnO film obtained commercially, J_{sc} of the solar cell increased strongly; finally, a 5.4% conversion efficiency was achieved.[25,26,28] Through introducing a light scattering layer composed of 600 nm-sized ZnO particles, Fujihara *et al.* also fabricated a double layer structured photoanode and obtained a conversion efficiency of 6.58%, which was the highest conversion efficiency for the DSCs based on ZnO photoanodes.[29]

Over the past decade, many technologies have been developed for the fabrication of ZnO photoanodes, such as physical or chemical vapor deposition, electrochemical deposition, sol–gel synthesis, hydrothermal or solvothermal growth, *et al.*[30–34] However, these methods are either technically demanding or needing high-temperature sintering to remove residual organic impurities, which can not help to reduce the energy pay-back time and fabricate flexible devices. Compared with these methods, direct precipitation process in aqueous solution is considered as an efficient way to synthesize ZnO particles with high purity and various shapes at low temperature. However, up to now, in quasi-solid state dye-sensitized solar cells, neither the controllable synthesis of ZnO in aqueous solution nor systematic investigation of the corresponding photoanodes' characteristics has been carried out.

Herein, through rapid precipitation, we reported the controllable synthesis of ZnO spindles with different sizes by varying the reactants concentration. Two samples were synthesized and SEM results showed that the average length of spindles was

Key Lab of Organic Optoelectronics and Molecular Engineering of Ministry of Education, Department of Chemistry, Tsinghua University, Beijing, P.R.China. E-mail: chldwang@mail.tsinghua.edu.cn
† Y.T. Shi and H. P. Dong contribute equally to this work.

Table 1 Differences of the synthesis conditions for the samples[a]

Sample	$Zn(OAc)_2 \cdot 2H_2O$ [g]	Ammonia [mL]
sample 1	1.8	5.0
sample 2	3.6	10.0

[a] Two samples were synthesized in 500 mL aqueous solution, in which the ratio of precursor and precipitant were maintained for all samples.

significantly increased by doubling the reactants concentration. Pore distributions, specific area, light scattering and electron transport of the corresponding photoanodes were investigated in detail. Furthermore, to combine the advantages of different sized ZnO particles, composite photoanodes were fabricated by mixing two samples together at a certain ratio.

2. Results and discussion

2.1 Preparation of ZnO spindles

The method to synthesise ZnO spindles controllably was similar to the method we reported before.[35] But through pouring the zinc source into the ammonia aqueous solution fast, the size of the spindles synthesized was in a narrow range. This will be discussed further in SEM and XRD results. Two samples were synthesized here. The precursor and precipitant were zinc acetate dihydrate and ammonia, respectively (see Table 1). The precipitation process was carried out at 70 °C for 1 h in an aqueous solution. The white precipitation was then filtered and washed with absolute alcohol, and the resulting product was also dispersed into deionized water for the preparation of the ZnO colloid paste. Finally, the doctor-blade technique was used to fabricate the ZnO film with the thickness being controlled by a 90 μm-thick tape on an FTO glass. The film was then thermal treated at 200 °C for 1 h. The assemble of the solar cells was similar to our previous report.[36]

2.2 SEM and XRD studies

Two samples were studied in our work. Compared with sample 1, sample 2 was synthesized by doubling the reactants concentration without changing other conditions. Fig. 1 showed the SEM images of sample 1 and sample 2. It could be easily found that with the reactants concentration doubling, the size of the sample increased obviously. From Fig. 1, we could see that in sample 1, the spindles were not quite intact; there were a lot of semi-spindles. Going with the size increase, spindles in sample 2 became more intact and some flower-like particles appeared, which had been also been observed by Gao.[37]

According to previous reports, formation of ZnO spindles in aqueous solution under direct precipitation process includes three steps. Firstly, the formation and growth of nanosized monocrystal; then half-spindle was formed through oriented aggregation of nanocrystals obtained in the first step; and at last an intact spindle was formed through the germination of a second half at its base.[37–40] Therefore, ZnO particles in the samples were doubtlessly polycrystalline. In this paper, XRD patterns were used to investigate the characteristic of the monocrystalline in the samples. From Fig. 2, we can see that

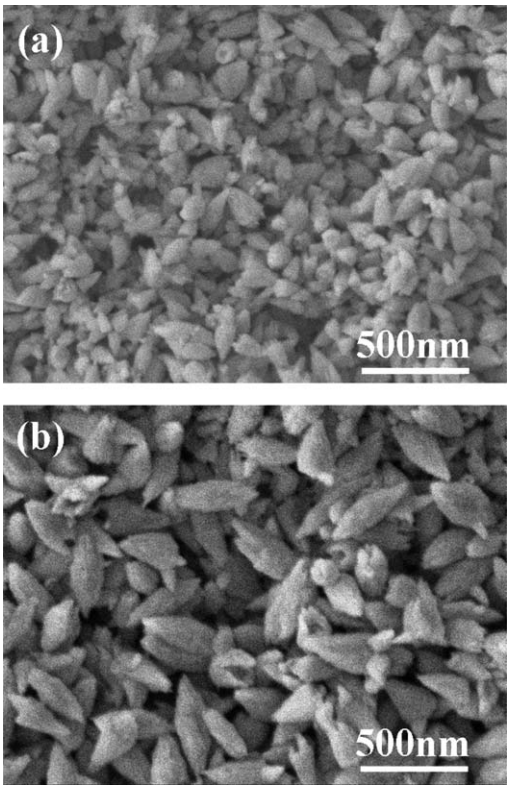

Fig. 1 SEM images of ZnO particles prepared at different reactants concentrations: a) sample 1; b) sample 2.

there were hardly any differences in the XRD patterns of two samples, indicating that reactants concentration had no influence on the characteristic of the monocrystalline formed in the first step. Therefore, it was considered that differences of the particles' sizes and morphologies might originate from the second and third step. At lower reactants concentrations as in the case of sample 1, number of as-synthesized monocrystallines was so finite that intact spindles could be hardly formed, also, size of their aggregated semi-spindles was smaller. At higher reactants concentrations such as sample 2, larger sized and more integrated ZnO spindles were easy to be obtained due to massive as-synthesized monocrystals.

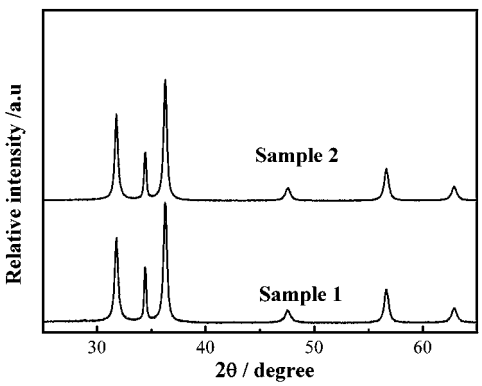

Fig. 2 X-ray diffraction (XRD) patterns of sample 1 and sample 2.

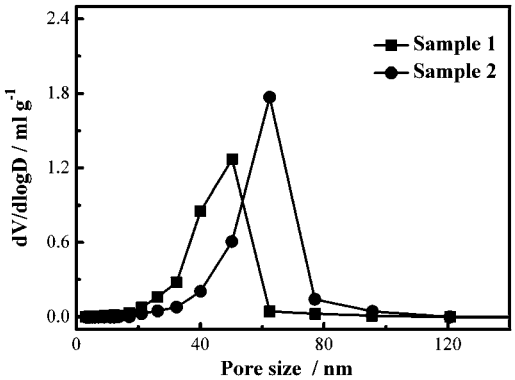

Fig. 3 Pore size distributions of sample 1 and sample 2.

2.3 Specific area and pore distribution

N_2 adsorption/desorption and mercury porosimeter method were used to detect the specific area and pore diameter of the photoanodes based on two samples, respectively; the results are shown in Fig. 3 and Table 2. We can see that as the reactants concentration increases, specific areas of the samples decreased form 20.48 m^2 g^{-1} to 17.41 m^2 g^{-1}, and the characteristic pore diameter increased from 50.3 nm to 62.4 nm, in accordance with their particle sizes. Worth mentioning is that characteristic pores of both samples were above 50 nm, far bigger than the photoanodes usually reported.[41] We all knew that the bigger the pores were, the easier is would be for electrolytes to penetrate, so our photoanodes were quite suitable to fabricate quasi-solid and even all-solid state DSCs.

2.4 Light scattering

To increase the probability of incident photons being absorbed, efficient light scattering is necessary for highly performed photoanodes in DSCs. For this purpose, sub-micrometre-sized particles which have a better light scattering ability for visible light or light scattering layer were usually introduced into photoanodes.[17,42,43] In this paper, light-scattering characterization of the samples was carried out in a UV-vis spectrophotometer equipped with an integrating sphere. Diffuse transmission can reveal the extent that the incident light is scattered by particles in the photoanode while the mirror transmission represents how much incident light passes through the photoanode without being scattered. The ideal light scattering activities of the photoanode should have a higher diffuse transmission and lower mirror transmission.

In Fig. 4 (a), it could be clearly seen that, with size of the particles increasing, diffuse transmission abilities enhanced from sample 1 to sample 2 in the spectral range between 400 nm~800 nm, quite in accordance with the particles' size. It revealed that large-sized ZnO spindles performed better than those smaller ones, beneficial to increasing the photons' probability being captured and the subsequent photocurrent. Fig. 4 (b) shows the mirror transmission curves of the two samples; it revealed that the extent incident light passing through the photoanode by mirror transmission decreased as the particle sizes increased with the reactants concentration. Transmission results in Fig. 4 indicate that, with increasing the particle sizes, incident light could be scattered efficiently. As we all know, how to make full use of the infrared or near-infrared light is still a challenge for the DSCs,

Table 2 Specific area and characteristic pore diameter of sample 1 and sample 2

Sample	Specific area (m^2g^{-1}) (N_2 sorption/desorption)	Characteristic pore diameter (nm) (mercury porosimeter)
Sample 1	20.48	50.3
Sample 2	17.41	62.4

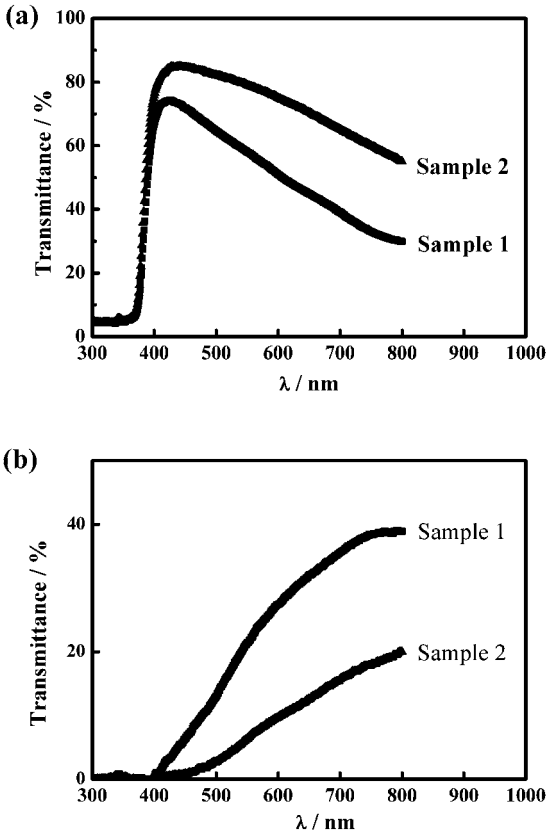

Fig. 4 Transmission curves of the samples: a) diffuse transmission; b) mirror transmission.

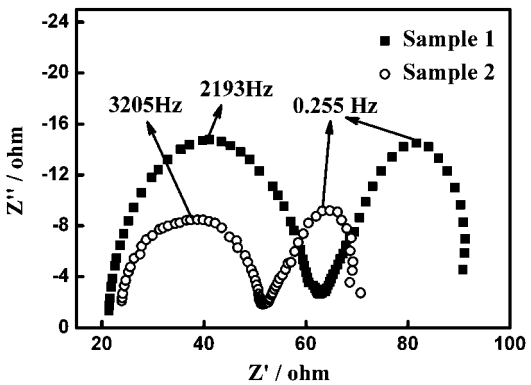

Fig. 5 Nyquist plots from EIS results for DSCs devices based on sample 1 and sample 2.

for the photoanodes in this work, not only visible light could be scattered, also near-infrared light could be scattered sufficiently by those ZnO spindles with a bigger size, well establishing a foundation for the future infrared or near-infrared sensitizers.

2.5 Electron transport

To investigate electron transport properties of these photoanodes composed of spindles with different sizes, Electrochemical Impedance Spectra (EIS) and Intensity Modulated Photocurrent Spectroscopy (IMPS) techniques were used to characterize our quasi-solid state DSC devices based on sample 1 and sample 2. In our experiment, EIS measurement was carried out on a electrochemical working station (CHI660, USA) with the signal frequency range from 0.05 Hz to 100 KHz under 0.5 sun light. As can be seen in Fig. 5, the Nyquist plot for each sample was composed of two semicircles. Based on previous reports, diameters of these two semicircles can represent the electron transport resistance in porous photoanode and the bulk resistance of the electrolyte according to their characteristic frequencies, respectively.[44] Compared with the device based on sample 1, the one based on sample 2 had a much smaller electron transport resistance, suggesting that electrons could transport much faster in porous photoanode composed of spindles with larger sizes. IMPS test was carried out on an IM6e electrochemical work station with a light wavelength of 530 nm, and the results were shown in Fig. 6. For each sample, the electron diffusion coefficient increased with enhancing light intensities, suggesting electrons could move faster at higher light intensity. This was because massive photoinduced electrons at higher light intensities could fill traps in the photoanodes sufficiently and thus facilitate the electron transport.[45] In Fig. 6, D_n values in devices based on sample 2 was much higher than the one based on sample 1 at the same light intensity. Generally, for a given photoinduced electron, it had to pass through numerous particles and their boundaries before being collected by the conductive substrate.[46] Therefore, morphology, interconnection between adjacent particles, specific area and porosity of the photoanode had great influence on the electron transport properties.[47–49] For the photoanode composed of larger-sized particles, electrons will transport faster due to its larger contact area between adjacent particles and less trap sites caused by a smaller specific area, just as comparing sample 2 with sample 1.

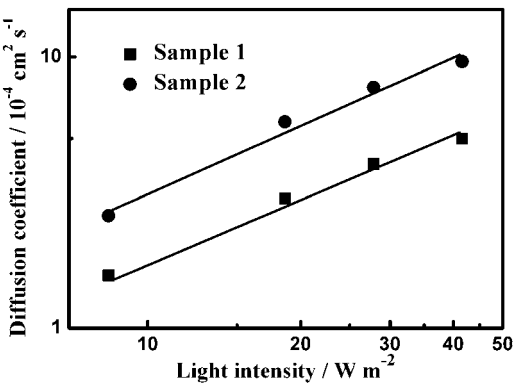

Fig. 6 Electron diffusion coefficient obtained from IMPS for sample 1 and sample 2.

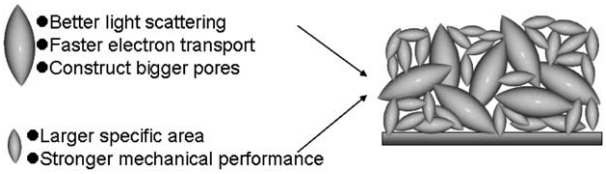

Fig. 7 Schematic diagram of the composite photoanode composed of spindles with different sizes.

2.6 Composite photoanodes

Since ZnO spindles with different sizes had their own advantages on specific area, pore-forming, light scattering and electron transport, *etc.*, a good idea for composited photoanodes with high performance was proposed through taking advantage of different sized spindles. As shown in Fig. 7, a simple strategy to realize this destination was to mix our ZnO spindles with two different sizes, in this way weight ratios of the different-sized particles could be controlled accurately. By the way, although our previous photoanodes based on polydisperse ZnO spindles have showed better PV performance under this conception,[33] yet size distributions of the spindles could hardly be controlled accurately, quite unfavourable to elucidate the relationship between the photoanode nanostructures and enhanced properties of DSCs. The SEM image of the composite photoanode containing 66.6%(w/w) sample 1 and 33.3%(w/w) samples 2 was shown in Fig. 8. We can see that large particles were evenly distributed in the small particles just as expected.

Photovoltaic performance of the devices based on sample 1, sample 2 and their composite photoanode were shown in Fig. 9 and the detailed results under AM 1.5 irradiation (100 mW cm^{-2} and 50 mW cm^{-2}) were listed in Table 3. Though sample 2 had a better light scattering ability and could transport electrons more freely, its corresponding photoanode showed a lower J_{sc} value and conversion efficiency than the one based on sample 1. In fact, except for light scattering and electron transport, other properties also had remarkable effects on the J_{sc} and conversion efficiency, especially the surface area of the photoanode. As aforementioned, the average particle size of sample 1 was smaller than that of sample 2, obviously, it could be regarded that a larger surface area for sample 1 was dominant and finally

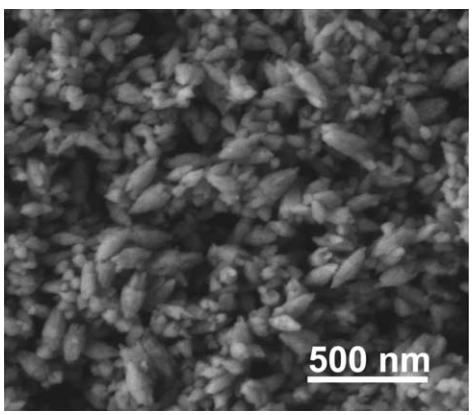

Fig. 8 SEM image of the composite photoanode containing 66.7%(w/w) sample 1 and 33.3%(w/w) sample 2.

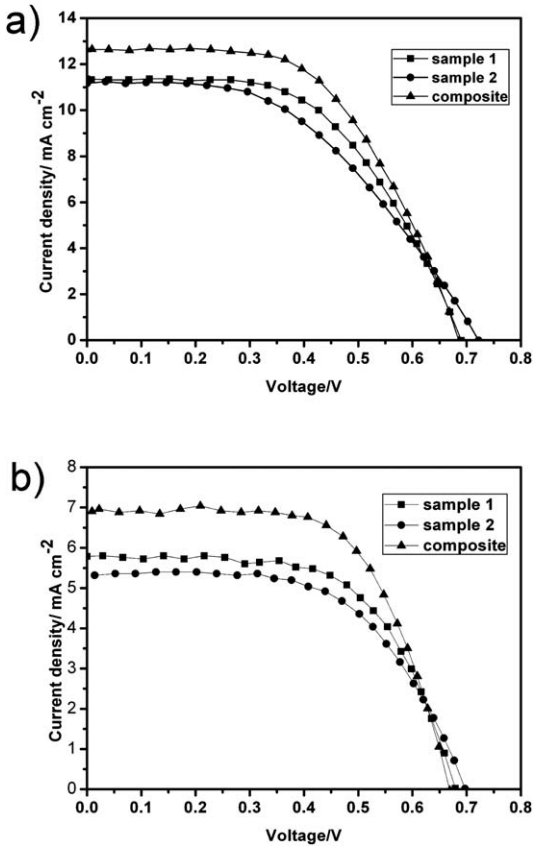

Fig. 9 Photovoltage performance of the solar cells based on sample 1, sample 2 and composite photoanode. a) under 1.0 sun; b) under 0.5 sun.

resulted in more sufficient dye-loading so as to generate more photoelectrons and a subsequently higher J_{sc} value. It was also clearly indicated that, the composite photoanode showed a better photovoltaic performance than those two with single dimensions. Also, as can be seen in Table 3, the improved conversion efficiency stemmed from the enhanced J_{sc} value and a better fill factor (FF). According to discussions aforesaid, better light scattering and electron transport advantages of larger sized sample 2 probably contributed to the increased J_{sc} and the subsequent conversion efficiency since photons were more apt to be harvested and the collection of photon-generated electrons were improved. Besides increasing the light scattering ability, large spindles could also introduce large pores inside the photoanode and thus facilitate penetration of our highly viscous PEO-based polymer gel electrolyte.[50] With large sized pores, electrolytes could soak into the photoanode more easily, obviously dye molecules could be regenerated in time. Compared with the device based on sample 2, the device based on composite photoanode had a higher fill factor (FF). It was thought that connection of the larger sized particles was improved since these small sized ones could serve as binder when being located among them. The improved connection was beneficial to the collection of electrons since their pathway to the conducting substrate was shortened and subsequent attenuation of charge recombination was obtained.

Table 3 Photovoltaic performances of DSCs based on sample 1, 2 and composite photoanode under AM 1.5 irradiation

Light intensity	Sample	J_{SC} /mA cm^{-2}	V_{OC} /V	F.F.	η/%
1.0 sun	sample 1	11.36	0.69	0.55	4.28
	sample 2	11.16	0.72	0.47	3.84
	composite	12.64	0.69	0.56	4.84
0.5 sun	sample 1	5.88	0.68	0.61	4.89
	sample 2	5.48	0.70	0.58	4.46
	composite	6.92	0.67	0.64	5.94

3. Conclusions

In summary, by altering reactants concentration, ZnO (semi-)-spindles with different sizes were controllably prepared through fast precipitation processes in aqueous solution. Photoanodes based on ZnO spindles with different sizes were fabricated at low sintering temperature (200 °C). Specific area, macropore structure, light scattering, and electron transport properties of these photoanodes composed of ZnO spindles with a certain size were systematically investigated by BET, Mercury porosimeter, Electrochemical Impedance Spectra (EIS), Intensity Modulated Photocurrent Spectroscopy (IMPS), respectively. Results showed that photoanodes based on small spindles had a larger specific area for dye loading and photoanodes based on large spindles had bigger pores, better light scattering and faster electron transport ability. Finally, composite photoanodes were made by mixing different sized spindles in fixed proportion. Photovoltaic performances of quasi-solid state DSCs based on composite photoanodes and photoanodes of single-sized spindles were studied. Without obvious decrease in open-circuit voltage and fill factor, the short-circuit photocurrent density of the DSCs based on composite photoanodes increased obviously and consequently a higher light-to-electrical conversion efficiency was achieved.

4. Experimental

Synthesis of single sized ZnO particles and fabrication of photoanode

ZnO spindles were synthesized in aqueous solution, and all reactants were used without further purification. Firstly, ammonia (28wt% of NH_3) was added into 500 mL distilled water under strong stirring. After the solution became homogeneous, zinc acetate dihydrate solution was poured into it quickly, 1 h later, the resulting white precipitation was filtered and washed with absolute alcohol. The ZnO paste was prepared by mixing ZnO power with distilled water (ZnO: water = 1 : 3), then followed ultrasonic and mechanical shock until the particles were dispersed homogeneously. In our experiment, doctor blade technique was used to prepare porous ZnO layer with the thickness being controlled by a 90 μm adhesive tape.

Assembly of the DSCs

The ZnO photoanode was sintered at certain temperature, then sensitized in 0.3 mM N719 absolute ethanol solution for 80 min, followed by cleaning with absolute ethanol. A chemically platinized conductive glass was used as the counter electrode. The composition of the polymer gel electrolyte: 0.1M LiI, 0.1M I_2, 0.6M 1,2-dimethyl-3-propyl imidazolium iodide, 0.45M

N-methyl-benzimidazole, and the solvent was 3-methoxy-propionitrile, PEO ($M_w = 2 \times 10^6$ g mol^{-1}) weight ratio (*vs.* liquid electrolyte) was 10%. When assembling DSC, the polymer gel electrolyte was sandwiched by a sensitized ZnO electrode and a counter electrode with two clips, the space between two electrode is controlled by an adhesive tape with a thickness of 30 μm and the DSC was not sealed. Finally, the DSC was baked at 80 °C to ensure the polymer gel electrolyte can penetrate into the nanoporous electrode.

Characterisation

Morphologies of the ZnO particles and the photoanodes were characterized by SEM technique (JSM 7401). The photovoltaic performance of the DSC were measured by KEITHLEY 4200 under solar simulator (Xenon lamp, Oriel, AM 1.5 100 mW cm^{-2}), and the incident light intensity was calibrated with standard crystalline silicon solar cell. The total active area of the DSC is 0.25 cm^2. Besides, macropore structure, light scattering, EIS and IMPS were investigated by AutoScan-3 Mercury porosimeter, HITACHI Model U-3010UV-vis spectrophotometer, CHI 660 electrochemical workstation, ZAHNER ENNIUM electrochemical workstation, respectively.

Acknowledgements

This work was supported by the National Natural Science Foundation of China under Grant No.50873055 and the National Key Basic Research and Development Program of China under Grant No.2009CB930602.

Notes and References

1 B. O'Regan and M. Grätzel, *Nature*, 1991, **353**, 737.
2 M. K. Nazeeruddin, F. D. Angelis, S. Fantacci, A. Selloni, G. Viscardi, P. Liska, S. Ito, B. Takeru and M. Grätzel, *J. Am. Chem. Soc.*, 2005, **127**, 16835.
3 Q. F. Zhang, C. S. Dandeneau, X. Y. Zhou and G. Z. Cao, *Adv. Mater.*, 2009, **21**, 4087.
4 M. Matsumura, S. Matsudaira and H. Tsubomura, *Ind. Eng. Chem. Prod. Res. Dev.*, 1980, **19**, 415.
5 G. Redmond, D. Fitzmaurize and M. Grätzel, *Chem. Mater.*, 1994, **6**, 686.
6 H. Rensmo, K. Keis, H. Lindström, S. Södergren, A. Solbrand, A. Hagfeldt, S.-E. Lindquist, L. N. Wang and M. Muhammed, *J. Phys. Chem. B*, 1997, **101**, 2598.
7 K. Keis, E. Magnusson, H. Lindström, S.-E. Lindquist and A. Hagfeldt, *Sol. Energy Mater. Sol. Cells*, 2002, **73**, 51.
8 A. B. F. Martinson, J. W. Elam, J. T. Hupp and M. J. Pellin, *Nano Lett.*, 2007, **7**, 2183.
9 E. Galoppini, J. Rochford, H. H. Chen, G. Saraf, Y. C. Lu, A. Hagfeldt and G. J. Boschloo, *J. Phys. Chem. B*, 2006, **110**, 16159.
10 M. Guo, P. Diao, X. D. Wang and S. M. Cai, *J. Solid State Chem.*, 2005, **178**, 3210.
11 M. Law, L. E. Greene, J. C. Johnson, R. Saykally and P. D. Yang, *Nat. Mater.*, 2005, **4**, 455.
12 J. B. Baxtera and E. S. Aydil, *Sol. Energy Mater. Sol. Cells*, 2006, **90**, 607.
13 D. I. Suh, S. Y. Lee, T. H. Kim, J. M. Chun, E. K. Suh, O. B. Yang and S. K. Lee, *Chem. Phys. Lett.*, 2007, **442**, 348.
14 W. G. Yang, F. R. Wan, Q. W. Chen, J. J. Li and D. S. Xu, *J. Mater. Chem.*, 2010, **20**, 2870.
15 D. H. Chen, F. Z. Huang, Y. B. Cheng and R. A. Caruso, *Adv. Mater.*, 2009, **21**, 2206.
16 Z. S. Wang, H. Kawauchi, T. Kashima and H. Arakawa, *Coord. Chem. Rev.*, 2004, **248**, 1381.
17 T. Hasobe, H. Imahori, S. Fukuzumi and P. V. Kamat, *J. Mater. Chem.*, 2003, **13**, 2515.
18 K. Zhu, N. R. Neale, A. Miedaner and A. J. Frank, *Nano Lett.*, 2007, **7**, 69.
19 A. Usami, *Chem. Phys. Lett.*, 1997, **277**, 105.
20 L. Schmidt-Mende and M. Grätzel, *Thin Solid Films*, 2006, **500**, 296.
21 B. Chi, L. Zhao, J. Li, J. Pu, Y. Chen, C. C. Wu and T. J. Jin, *J. Nanosci. Nanotechnol.*, 2008, **8**, 3877.
22 K. J. Jiang, T. Kitamura, Y. Wada and S. Yanagida, *Bull. Chem. Soc. Jpn.*, 2003, **76**, 2415.
23 E. Hosono, S. Fujihara and T. Kimura, *Electrochim. Acta*, 2004, **49**, 2287.
24 K. Kakiuchi, E. Hosono and S. Fujihara, *J. Photochem. Photobiol., A*, 2006, **179**, 81.
25 T. P. Chou, Q. F. Zhang, G. E. Fryxell and G. Z. Cao, *Adv. Mater.*, 2007, **19**, 2588.
26 Q. F. Zhang, T. P. Chou, B. Russo, S. A. Jenekhe and G. Z. Cao, *Angew. Chem., Int. Ed.*, 2008, **47**, 2402.
27 F. Xu, M. Dai, Y. N. Lu and L. T. Sun, *J. Phys. Chem. C*, 2010, **114**, 2776.
28 Q. F. Zhang, T. P. Chou, B. Russo, S. A. Jenekhe and G. Z. Cao, *Adv. Funct. Mater.*, 2008, **18**, 1654.
29 M. Saito and S. Fujihara, *Energy Environ. Sci.*, 2008, **1**, 280.
30 P. D. Yang, H. Q. Yan, S. Mao, R. Russo, J. Johnson, R. Saykally, N. Morris, J. Pham, R. R. He and H. J. Choi, *Adv. Funct. Mater.*, 2002, **12**, 323.
31 X. D. Wang, Y. Ding, C. J. Summers and Z. L. Wang, *J. Phys. Chem. B*, 2004, **108**, 8773.
32 M. Fu, Zhou, Q. F. Xiao, B. Li, R. L. Zong, W. Chen and J. Zhang, *Adv. Mater.*, 2006, **18**, 1001.
33 M. Vafaee and M. S. Ghamsari, *Mater. Lett.*, 2007, **61**, 3265.
34 Y. C. Qiu, W. Chen and S. H. Yang, *J. Mater. Chem.*, 2010, **20**, 1001.
35 Y. T. Shi, C. Zhan, L. D. Wang, B. B. Ma, R. Gao, Y. F. Zhu and Y. Qiu, *Adv. Funct. Mater.*, 2010, **20**, 437.
36 Y. Geng, Y. T. Shi, L. D. Wang, B. B. Ma, R. Gao, Y. F. Zhu, H. P. Dong and Y. Qiu, *Phys. Chem. Chem. Phys.*, 2011, DOI: 10.1039/C0CP01866J.
37 X. D. Gao, X. M. Li and W. D. Yu, *J. Phys. Chem. B*, 2005, **109**, 1155.
38 Q. P. Zhong and E. Matijevic, *J. Mater. Chem.*, 1996, **6**, 443.
39 M. Öner, J. Norwig, W. H. Meyer and G. Wegner, *Chem. Mater.*, 1998, **10**, 460.
40 A. P. A. Oliveira, J. F. Hochepied, F. Grillon and M. H. Berger, *Chem. Mater.*, 2003, **15**, 3202.
41 B. Z. Tian, F. Y. Li, Z. Q. Bian, D. Y. Zhao and C. H. Huang, *J. Mater. Chem.*, 2005, **15**, 2414.
42 G. Lozano, S. Colodrero, O. Caulier, M. E. Calvo and H. Miguez, *J. Phys. Chem. C*, 2010, **114**, 3681.
43 A. Mihi and H. Miguez, *J. Phys. Chem. B*, 2005, **109**, 15968.
44 Q. Wang, J. E. Moser and M. Gratzel, *J. Phys. Chem. B*, 2005, **109**, 14945.
45 K. Schwarzburg and F. Willig, *Appl. Phys. Lett.*, 1991, **58**, 2520.
46 K. D. Benkstein, N. Kopidakis, J. V. D. Lagemaat and A. J. Frank, *J. Phys. Chem. B*, 2003, **107**, 7759.
47 M. J. Cass, F. L. Qiu, A. B. Walker, A. C. Fisher and L. M. Peter, *J. Phys. Chem. B*, 2003, **107**, 113.
48 S. Nakade, Y. Saito, W. Kubo, T. Kitamura, Y. Wada and S. Yanagida, *J. Phys. Chem. B*, 2003, **107**, 8607.
49 J. V. D. Lagemaat, K. D. Benkstein and A. J. Frank, *J. Phys. Chem. B*, 2001, **105**, 12433.
50 Y. T. Shi, C. Zhan, L. D. Wang, B. B. Ma, R. Gao, Y. F. Zhu and Y. Qiu, *Phys. Chem. Chem. Phys.*, 2009, **11**, 4230.

